1-1-2014

The impact of carbon sp(2) fraction of reduced graphene oxide on the performance of reduced graphene oxide contacted organic transistors

Narae Kang
University of Central Florida

Saiful I. Khondaker
University of Central Florida

The impact of carbon sp^2 fraction of reduced graphene oxide on the performance of reduced graphene oxide contacted organic transistors

Cite as: Appl. Phys. Lett. **105**, 223301 (2014); https://doi.org/10.1063/1.4902881
Submitted: 20 July 2014 . Accepted: 16 November 2014 . Published Online: 01 December 2014

Narae Kang, and Saiful I. Khondaker

The impact of carbon sp^2 fraction of reduced graphene oxide on the performance of reduced graphene oxide contacted organic transistors

Narae Kang[1,2] and Saiful I. Khondaker[1,2,3,a)]
[1]*Nanoscience Technology Center, University of Central Florida, 12424 Research Parkway, Suite 400, Orlando, Florida 32826, USA*
[2]*Department of Physics, University of Central Florida, 12424 Research Parkway, Suite 400, Orlando, Florida 32826, USA*
[3]*School of Electrical Engineering and Computer Science, University of Central Florida, 12424 Research Parkway, Suite 400, Orlando, Florida 32826, USA*

(Received 20 July 2014; accepted 16 November 2014; published online 1 December 2014)

One of the major bottlenecks in fabricating high performance organic field effect transistors (OFETs) is a large interfacial contact barrier between metal electrodes and organic semiconductors (OSCs) which makes the charge injection inefficient. Recently, reduced graphene oxide (RGO) has been suggested as an alternative electrode material for OFETs. RGO has tunable electronic properties and its conductivity can be varied by several orders of magnitude by varying the carbon sp^2 fraction. However, whether the sp^2 fraction of RGO in the electrode affects the performance of the fabricated OFETs is yet to be investigated. In this study, we demonstrate that the performance of OFETs with pentacene as OSC and RGO as electrode can be continuously improved by increasing the carbon sp^2 fraction of RGO. When compared to control palladium electrodes, the mobility of the OFETs shows an improvement of ~200% for 61% sp^2 fraction RGO, which further improves to ~500% for 80% RGO electrode. Similar improvements were also observed in current on-off ratio, on-current, and transconductance. Our study suggests that, in addition to π-π interaction at RGO/pentacene interface, the tunable electronic properties of RGO electrode have a significant role in OFETs performance. © *2014 AIP Publishing LLC*.
[http://dx.doi.org/10.1063/1.4902881]

Organic field-effect transistors (OFETs) have received much attention due to their potential applications in low-cost, light-weight, and large-area flexible electronic devices.[1–4] A major challenge in improving OFET device performance is to reduce the large interfacial barrier between metal and organic semiconductors (OSCs), which results in a low charge injection from the metal electrode to OSC and limits the performance of OFETs.[5–10] The large interface barrier can be originated from discontinuity in morphology, interfacial dipole barrier, and Schottky barrier. In order to address the challenge of low charge injection, reduced graphene oxide (RGO) has been introduced as a promising electrode for OFETs due to its high work function and strong π-π interaction with organic molecules which can reduce the injection barrier at the electrode/organic interface.[11–16] In addition, its solution-processing method to produce graphene sheets in large quantities at low cost and compatibility with various substrates including plastics, makes them attractive for fabrication of OFETs. It has been shown that RGO consists of sp^2 graphene domains surrounded by a continuous matrix of sp^3 networks, which contains oxygen functional groups such as hydroxyl, epoxy, and carboxyl.[17,18] Interestingly, the ratio of sp^2/sp^3 fractions, can be tuned by controlling the reduction condition giving rise to tunable electronic and optical properties. Such sp^2 fraction tuning can also lead to a variation of work function and bandgap of RGO.[18–24] However, how the variation of carbon sp^2 fraction of RGO will affect the performance of RGO-contacted OFETs remains unexplored.

In this paper, we present a systematic study of the electrical transport properties of pentacene field-effect transistors (FETs) using RGO of various reduction efficiency as electrodes. RGO sheets of different carbon sp^2 fraction varying from 61% to 80% were synthesized by reducing the individual graphene oxide (GO) sheets via hydrazine hydrate method and by varying the reduction time from 10 min to 60 min. The RGO sheets were assembled between prefabricated palladium (Pd) patterns via dielectrophoresis (DEP). The RGO electrodes of 2 μm × 25 μm were defined by electron beam lithography (EBL) and subsequent oxygen plasma etching. A control Pd contacted pentacene FETs was also fabricated for comparison. From the electronic transport measurements of 40 devices, we show that the average saturation mobility (μ) increased from 0.06 for Pd electrodes to 0.11, 0.20, and 0.31 cm^2/V s for RGO electrodes with a sp^2 fraction (reduction time) of 61% (10 min), 66% (30 min), and 80% (60 min), respectively. In addition, current on-off ratio (I_{on}/I_{off}), the magnitude of on-current ($|I_{on}|$), and transconductance (g_m) show similar improvements with increasing the sp^2 fraction. This demonstrates that, although a few minutes of reduction (10 min, 61% sp^2 fraction) of RGO electrodes can improve the OFET device performance by 200% compared to bare Pd electrode, significant improvements of up to 500% can be achieved by further increasing the reduction efficiency (up to 60 min, 80% sp^2 fraction) of RGO electrode. We discuss the improvements from work function and conductivity consideration of RGO. Our study

a)Author to whom correspondence should be addressed. Electronic mail: saiful@ucf.edu

suggests that the tunable electronic properties of RGO can have significant impact on the performance of RGO contacted OFETs.

The individual GO sheets were obtained from commercial sources and the RGO sheets of different reduction efficiency were produced via chemical reduction in hydrazine hydrate for either 10, 30, or 60 min at 90 °C as described in our previous publication.[21] The carbon sp^2 fraction was calculated as 61%, 66%, and 80% for 10, 30, and 60 min of reduction time of RGO sheets, respectively. The carbon sp^2 fraction was obtained by taking the ratio of the integrated peak areas corresponding to the *C-C* peak, to the total area under the *C* 1*s* spectrum from the X-ray photoelectron spectroscopy (XPS) (Figure S1 in the supplementary material).[21,25]

Devices were fabricated on doped silicon (Si)/silicon dioxide (SiO_2) substrates. The RGO sheets of different sp^2 fractions were assembled between Pd patterns of $5\,\mu m \times 25\,\mu m$ via DEP.[26] In our previous study,[26] we focused on a few RGO flakes assembly in a short channel. Here, we optimized the DEP assembly technique to obtain a thin RGO film in large channel geometry. We used an AC voltage of 5 V with a 1 MHz frequency for 30 s. Figure 1(a) shows a representative scanning electron microscopy (SEM) image of RGO assembled between Pd. The image was taken using a Zeiss Ultra 55 SEM with an in-lens secondary electron detector at 1.2 kV. The average thickness of the film is ~20 nm determined by the atomic force microscopy (AFM) study (see supplementary material, Figure S2).[25] The representative current-voltage (I_d-V_d) characteristics of the assembled RGO sheets with different reduction efficiency are shown in Figure 1(b). The increase in carbon sp^2 fraction resulted in a decrease of room-temperature resistance (R). The average two-terminal R is 20.5 MΩ, 702 kΩ, and 165 kΩ for RGO sheets with carbon sp^2 fraction of 61% (green square), 66% (blue triangle), and 80% (red circle) (Figure 1(c)). The decrease of resistance with increasing sp^2 fraction demonstrates that the restoration of π-π bond improves charge percolation pathways in the RGO sheets.[20,21]

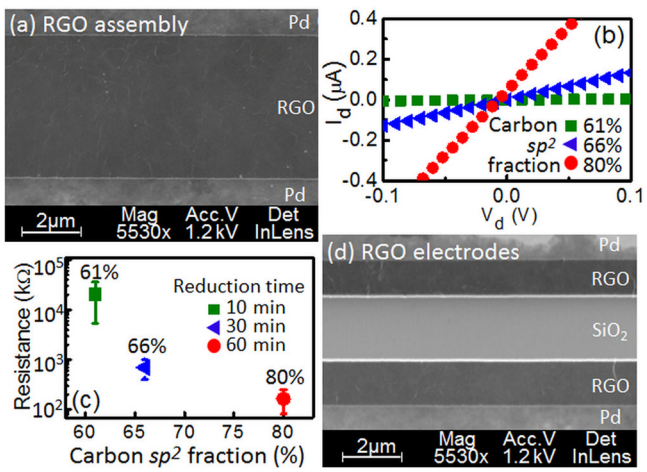

FIG. 1. (a) SEM images of DEP assembled RGO thin film and (b) Current-voltage (I_d-V_d) characteristics of RGO thin films containing different carbon sp^2 fraction. (c) Resistance of RGO films with different reduction time. Carbon sp^2 fractions are 61% (green square), 66% (blue triangle), and 80% (red circle) for 10, 30, and 60 min reduction time of RGO sheets. (d) SEM image of RGO electrodes after oxidative cutting.

The RGO electrodes of channel length (L) = 2 μm and channel width (W) = 25 μm were fabricated via spin coating of poly(methyl methacrylate) (PMMA), defining a $2\,\mu m \times 25\,\mu m$ window on RGO by EBL, and subsequent oxygen plasma etching for 2 min. Finally, the devices were kept into acetone for 3 h to remove the residual PMMA on the devices. The SEM image of the resulting RGO electrodes is shown in the Figure 1(d), showing well-defined channel dimension. A total of 30 devices using RGO electrodes were made, 10 devices for each sp^2 fraction. For control devices, we also fabricated 10 devices using bare Pd electrodes with the same dimension as RGO electrodes. All the samples were then loaded into a thermal evaporator for pentacene deposition. Pentacene (Sigma Aldrich, ≥99.9%) film with a thickness of 30 nm was then thermally deposited under the vacuum at a pressure of 2×10^{-6} mbars. In order to minimize the device-to-device fluctuation from the active materials morphology, all of the pentacene films were deposited under identical conditions. The morphological investigation carried out by an AFM shows that all the films have similar morphology with an average grain size of 350–500 nm (Figure S3).[25] The electrical measurements of all the devices were carried out in a probe station placed inside a glove box with an oxygen content of less than 0.5 ppm and the data was recorded using a HP 4145B semiconductor parameter analyzer.

Figures 2(a)–2(d) show the drain current (I_d) *vs* source-drain bias voltage (V_d) curves (output characteristics) at different gate-voltages (V_g) for our representative pentacene FET devices with Pd electrodes, and RGO electrodes of 61%, 66%, and 80% carbon sp^2 fraction, respectively. The V_g was varied from 0 to −20 V in a step of −5 V. All the devices show p-type FET behavior with a good gate modulation along with a linear behavior at low bias and a saturation behavior at higher bias voltage. For a clear comparison, we plotted all the curves in the same scale. From here, we observe that the magnitude of the output current of the pentacene FET increases with increasing sp^2 fraction of the RGO electrodes. The magnitude of the output current (at $V_d = -50$ V and $V_g = -20$ V) for Pd contact is 1.06 μA, while it is 2.62, 4.93, and 7.6 μA for the RGO electrode devices with 61%, 66%, and 80%, sp^2 fraction, respectively. The magnitude of the output current is more than 2 and 7 times higher for RGO electrodes with 61% and 80% sp^2 fraction, respectively, compared to the control Pd device. Since the morphology of all the devices is similar, the increase of output current with increasing RGO reduction efficiency clearly shows that the carbon sp^2 fraction of RGO has a significant impact on the output characteristics of the devices.

For further investigation of the effect of carbon sp^2 fraction of RGO electrodes on the device performance, we also measured the corresponding transfer curves (I_d *vs* V_g) of the same devices at saturation regime ($V_d = -50$ V) (Figures 2(e)–2(h)) and calculated μ, I_{on}/I_{off}, and $|I_{on}|$ of the devices. The mobility is calculated using the standard formula: $\mu = (2LI_{d,sat})/(WC_i(V_g - V_T)^2)$, where $I_{d,sat}$ is saturation current, C_i is the gate capacitance (13.8 nF/cm^2), and V_T is the threshold voltage. The values of μ for Pd, 61%, 66%, and 80% carbon sp^2 fraction of RGO are 0.052, 0.144, 0.205, and 0.319 cm^2/V s, respectively. This demonstrates that the

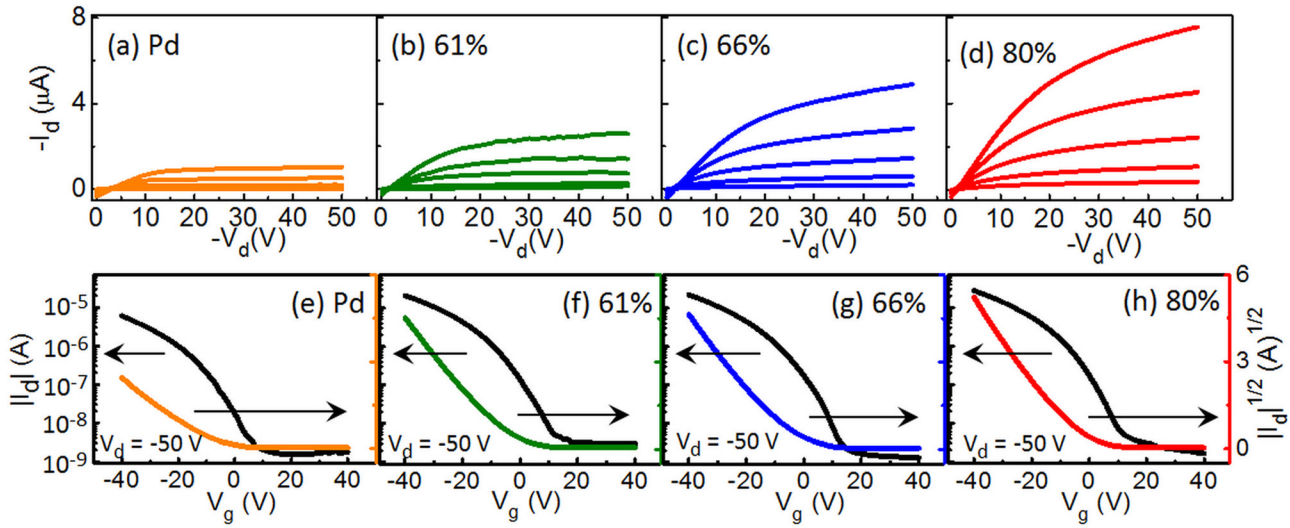

FIG. 2. Output characteristics (I_d-V_d) of pentacene transistors at $V_g = 0$, −5, −10, −15, and −20 V (bottom to top) for (a) Pd, (b) 61%, (c) 66%, and (d) 80% carbon sp^2 fraction RGO in the electrodes. Transfer characteristics (I_d-V_g) of pentacene transistors at $V_d = -50$ V (left axis) and $(I_d)^{1/2}$ (right axis) of the devices with (a) Pd, (b) 61%, (c) 66%, and (d) 80% carbon sp^2 fraction RGO in the electrodes.

mobility of the pentacene FETs also increases with increasing the carbon sp^2 fraction of RGO electrodes. The values of μ are 2.5 times higher for 61% RGO and 6 times higher for 80% RGO compared to the control Pd contacted device. The transfer curves also show that the I_{on}/I_{off} and $|I_{on}|$ (I_d at $V_g = -40$ V) increases with increasing carbon sp^2 fraction of RGO electrodes. The I_{on}/I_{off} and $|I_{on}|$ are 3.9×10^3 and 6.13 μA for the control Pd electrodes, 5.4×10^3 and 19.7 μA for 61% RGO electrodes, 1.7×10^4 and 24.2 μA for 66%, and 2.2×10^4 and 32.2 μA for 80% RGO electrodes. In addition, we have also extracted the transconductance ($g_m = dI/dV_g$) in the linear regime (at $V_d = -10$ V and $V_g = -40$ V) of the transfer curve (Figure S4).[25] The g_m was found to be 0.06 μS, 0.10 μS, 0.18 μS, and 0.23 μS for the control Pd, 61%, 66%, and 80% RGO electrodes, respectively. Therefore, μ, I_{on}/I_{off}, $|I_{on}|$, and g_m are improved significantly with increasing the carbon sp^2 fraction of RGO electrodes.

The characteristics measured from all the devices (10 in each category) are summarized in Figure 3 (see also Table S1),[25] where we plot the μ, I_{on}/I_{off}, $|I_{on}|$, and g_m as a function of the carbon sp^2 fraction of RGO electrodes. Figure 3 shows

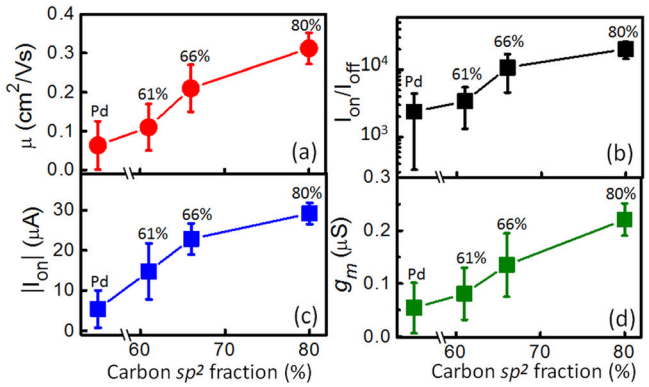

FIG. 3. Summary of OFET performance from 40 devices. (a) μ, (b) I_{on}/I_{off}, (c) $|I_{on}|$, and (d) g_m, for Pd electrode and RGO electrode of 61%, 66%, and 80% carbon sp^2 fraction.

that, similar to our representative devices, the average μ is increased from 0.06 for Pd to 0.11, 0.20, and 0.31 cm^2/V s for 61%, 66%, and 80% of RGO electrodes, respectively. The increase in the average μ for our OFETs is more than 5 times higher for 80% compared to the Pd contacted control devices. Similar significant increase can also be observed in the average value of the I_{on}/I_{off}, $|I_{on}|$, and g_m with increased reduction efficiency of RGO electrodes (Figures 3(b)–3(d)). For the control Pd electrode devices, the average value of I_{on}/I_{off}, $|I_{on}|$, and g_m are 2.4×10^3, 5.5 μA, and 0.05 μS, respectively. These values increased to 3.5×10^3 (1.5 times), 14.9 μA (3 times), and 0.08 μS (1.5 times) for 61%, 1.1×10^4 (4 times), 22.7 μA (4 times), and 0.14 μS (3 times) for 66%, and 2.1×10^4 (10 times), 29.3 μA (6 times), and 0.22 μS (4 times), for 80% of carbon sp^2 fraction in RGO electrodes. From this study, it is clear that the different reduction efficiency of RGO electrode, which controls the carbon sp^2 fraction, resistance, and work function of RGO, plays an important role in determining the performance of OFETs. Our study also demonstrates that, although a few minutes (10 min, 61%) of reduction efficiency of RGO electrodes can enhance the device performance compared to the control Pd contacted devices, the maximum performance is achieved using the highest reduction efficiency (60 min, 80%) of RGO electrodes.

Since all the devices have the same organic semiconductor as channel materials deposited under identical conditions, the variation in device performance should be related to the electrode materials and electrode/pentacene interface. If the interfacial Schottky barrier is φ_b, the current flowing through the device at a fixed bias voltage and temperature (T) can be approximated as $I_d \propto exp(-\Phi_b/kT)$,[27] where k is a Boltzmann constant. A decrease in Φ_B will result in an increased charge injection and higher device current. However, Φ_B is related to the work function difference between the pentacene and the electrode. The work function of Pd is 5.1 eV which is close to the highest occupied molecular orbital (HOMO) level of pentacene (5.0 eV). On the other hand, the typical work function of highly reduced RGO

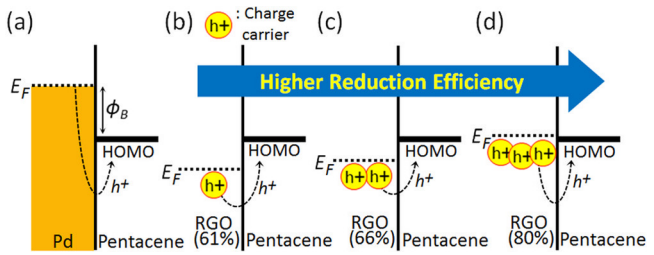

FIG. 4. Schematic of energy level diagrams of (a) Pd/pentacene, (b) 61% RGO/pentacene, (c) 66% RGO/pentacene, and (d) 80% RGO/pentacene. This figure shows Fermi level (E_F), HOMO level of pentacene, and ϕ_B.

is reported to be in the range of 4.6–5.0 eV,[12,13,16,24] close to the work function of conventional metal electrodes. Recently, Kumar *et al.*[23] reported that the work function of RGO can be further tuned up to ~7 eV by varying the degree of reduction (lower reduction has a higher work function). This suggests that the work function of 80% sp^2 fraction RGO is close to the HOMO level of pentacene, while the work function of 66% and 61% carbon sp^2 fraction of RGO should be higher than 5.0 eV.

Figure 4 shows the schematic diagram of the energy level for different reduction efficiency of RGO (with the carbon sp^2 fraction of 61%, 66%, and 80%), and Pd with pentacene. Even though the work function of Pd is very close to the HOMO level of pentacene, in Figure 4(a) we show a significant barrier between Pd and pentacene. This is due to the fact that when Pd is contacted with pentacene, the effective work function of Pd is significantly lowered due to large dipole barrier formation at Pd/pentacene interface known as the "push back effect."[8] This gives rise to a large Schottky barrier for hole injection at electrode/organic interface and causes an inferior device performance. In contrast, due to a strong π-π interaction existing at RGO/pentacene interface (organic–organic interface), significant dipole formation may not occur and the effective work function of RGO will not be significantly modified. In Figures 4(b), 4(c), and 4(d), we show the energy level diagrams for 61%, 66%, and 80% RGO electrodes, respectively. Based on this diagram, there are no hole injection barriers for 61% and 66% RGO, while the barrier for 80% RGO is negligible. Therefore, considering only the work function, one would have expected that the device performance for pentacene OFETs should be independent of the carbon sp^2 fraction of RGO electrode. This is in contrast to our experimental observation. Our results suggest that the carbon sp^2 fraction of RGO in the electrode, which tunes the conductivity of RGO, has a significant role in the OFET device performance. This can be understood from the charge carrier injection consideration. Even though all the RGO have favorable interfacial barriers, if the electrode does not have enough charge carriers to inject into the organic semiconductor, it cannot do an efficient carrier injection.[28] Since the conductivity of RGO depends upon the carbon sp^2 fraction and the conductivity of 61% RGO is two orders of magnitude lower than that of 80% RGO (Figure 1(c)), the 61% RGO does not have enough carrier to inject into pentacene, compared to 80% RGO. As a result, the 80% RGO contacted pentacene devices show the best device performance.

In conclusion, we investigated electron transport properties of pentacene FETs where RGO of different carbon sp^2 fraction (reduction efficiency) was used as electrodes. We found that, although the device performance such as mobility, current on-off ratio, on-current, and transconductance of all the RGO contacted devices show improvement compared to control Pd contacted devices, the best performance was achieved from the highest reduction efficiency RGO electrode. Since all the RGO electrodes have favorable work function for hole injection into pentacene, our study suggests that the tunable electronic properties of RGO is an important parameter that needs to be considered in fabricating RGO contacted organic devices.

This work was supported by U.S. National Science Foundation (NSF) under Grant No. ECCS 1102228.

[1]C. D. Dimitrakopoulos and P. R. L. Malenfant, Adv. Mater. **14**, 99 (2002).
[2]S. R. Forrest, Nature **428**, 911 (2004).
[3]B. Hu, L. Yan, and M. Shao, Adv. Mater. **21**, 1500 (2009).
[4]H. Klauk, Chem. Soc. Rev. **39**, 2643 (2010).
[5]L. Burgi, T. J. Richards, R. H. Friend, and H. Sirringhaus, J. Appl. Phys. **94**, 6129 (2003).
[6]S. Braun, W. R. Salaneck, and M. Fahlman, Adv. Mater. **21**, 1450 (2009).
[7]I. G. Hill, A. Rajagopal, A. Kahn, and Y. Hu, Appl. Phys. Lett. **73**, 662 (1998).
[8]N. Koch, A. Kahn, J. Ghijsen, J. J. Pireaux, J. Schwartz, R. L. Johnson, and A. Elschner, Appl. Phys. Lett. **82**, 70 (2003).
[9]D. J. Gundlach, L. Zhou, J. A. Nichols, T. N. Jackson, P. V. Necliudov, and M. S. Shur, J. Appl. Phys. **100**, 024509 (2006).
[10]D. Adil and S. Guha, J. Phys. Chem. C **116**, 12779 (2012).
[11]S. Pang, H. N. Tsao, X. Feng, and K. Muellen, Adv. Mater. **21**, 3488 (2009).
[12]H. A. Becerril, R. M. Stoltenberg, M. L. Tang, M. E. Roberts, Z. Liu, Y. Chen, D. H. Kim, B. L. Lee, S. Lee, and Z. Bao, ACS Nano **4**, 6343 (2010).
[13]P. H. Wobkenberg, G. Eda, D. S. Leem, J. C. de Mello, D. D. C. Bradley, M. Chhowalla, and T. D. Anthopoulos, Adv. Mater. **23**, 1558 (2011).
[14]C. G. Lee, S. Park, R. S. Ruoff, and A. Dodabalapur, Appl. Phys. Lett. **95**, 023304 (2009).
[15]K. Suganuma, S. Watanabe, T. Gotou, and K. Ueno, Appl. Phys. Express **4**, 021603 (2011).
[16]J. S. Lee, N. H. Kim, M. S. Kang, H. Yu, D. R. Lee, J. H. Oh, S. T. Chang, and J. H. Cho, Small **9**, 2817 (2013).
[17]S. Stankovich, D. A. Dikin, G. H. B. Dommett, K. M. Kohlhaas, E. J. Zimney, E. A. Stach, R. D. Piner, S. T. Nguyen, and R. S. Ruoff, Nature **442**, 282 (2006).
[18]K. P. Loh, Q. Bao, G. Eda, and M. Chhowalla, Nat. Chem. **2**, 1015 (2010).
[19]C. Mattevi, G. Eda, S. Agnoli, S. Miller, K. A. Mkhoyan, O. Celik, D. Mastrogiovanni, G. Granozzi, E. Garfunkel, and M. Chhowalla, Adv. Funct. Mater. **19**, 2577 (2009).
[20]G. Eda, Y. Y. Lin, C. Mattevi, H. Yamaguchi, H. A. Chen, I. S. Chen, C. W. Chen, and M. Chhowalla, Adv. Mater. **22**, 505 (2010).
[21]D. Joung and S. I. Khondaker, Phys. Rev. B **86**, 235423 (2012).
[22]D. Joung and S. I. Khondaker, J. Phys. Chem. C **117**, 26776 (2013).
[23]P. V. Kumar, M. Bernardi, and J. C. Grossman, ACS Nano **7**, 1638 (2013).
[24]B. Kang, S. Lim, W. H. Lee, S. B. Jo, and K. Cho, Adv. Mater. **25**, 5856 (2013).
[25]See supplementary material at http://dx.doi.org/10.1063/1.4902881 for XPS of RGO, AFM image of RGO electrode, pentacene film morphology, transfer curve in linear regime, and summary of all devices.
[26]D. Joung, A. Chunder, L. Zhai, and S. I. Khondaker, Nanotechnology **21**, 165202 (2010).
[27]B. K. Sarker and S. I. Khondaker, ACS Nano **6**, 4993 (2012).
[28]X. Ou, L. Jiang, P. Chen, M. Zhu, W. Hu, M. Liu, J. Zhu, and H. Ju, Adv. Funct. Mater. **23**, 2422 (2013).